

Experimental Quantum Switching for Exponentially Superior Quantum Communication Complexity

Kejin Wei,^{1,2,*} Nora Tischler,^{3,*} Si-Ran Zhao,^{1,2} Yu-Huai Li,^{1,2} Juan Miguel Arrazola,^{4,5}
Yang Liu,^{1,2} Weijun Zhang,⁶ Hao Li,⁶ Lixing You,⁶ Zhen Wang,⁶ Yu-Ao Chen,^{1,2} Barry
C. Sanders,^{1,7,8} Qiang Zhang,^{1,2} Geoff J. Pryde,³ Feihu Xu,^{1,2} and Jian-Wei Pan^{1,2}

¹*Shanghai Branch, Hefei National Laboratory for Physical
Sciences at Microscale and Department of Modern Physics,
University of Science and Technology of China, Shanghai, 201315, China*

²*CAS Center for Excellence and Synergetic Innovation
Center in Quantum Information and Quantum Physics,
University of Science and Technology of China, Shanghai 201315, P. R. China*

³*Centre for Quantum Dynamics, Griffith University, Brisbane, QLD 4111, Australia*

⁴*Xanadu, 372 Richmond Street W, Toronto, Ontario M5V 1X6, Canada*

⁵*Centre for Quantum Technologies, National University of Singapore,
3 Science Drive 2, Singapore 117543*

⁶*State Key Laboratory of Functional Materials for Informatics,
Shanghai Institute of Microsystem and Information Technology,
Chinese Academy of Sciences, Shanghai 200050, China*

⁷*Institute for Quantum Science and Technology,
University of Calgary, Alberta T2N 1N4, Canada*

⁸*Program in Quantum Information Science,
Canadian Institute for Advanced Research,
Toronto, Ontario M5G 1M1, Canada*

Abstract

Finding exponential separation between quantum and classical information tasks is like striking gold in quantum information research. Such an advantage is believed to hold for quantum computing but is proven for quantum communication complexity. Recently, a novel quantum resource called the quantum switch—which creates a coherent superposition of the causal order of events, known as quantum causality—has been harnessed theoretically in a new protocol providing provable exponential separation. We experimentally demonstrate such an advantage by realizing a superposition of communication directions for a two-party distributed computation. Our photonic demonstration employs d -dimensional quantum systems, qudits, up to $d = 2^{13}$ dimensions and demonstrates a communication complexity advantage, requiring less than (0.696 ± 0.006) times the communication of any causally ordered protocol. These results elucidate the crucial role of the coherence of communication direction in achieving the exponential separation for the one-way processing task, and open a new path for experimentally exploring the fundamentals and applications of advanced features of indefinite causal structures.

* These authors contributed equally to this work.

Computation by separated parties with minimal communication is the focus of communication complexity, which has applications to distributed computing, very-large-scale integration, streaming algorithms, and more [1]. For quantum information, communication complexity is especially exciting as exponential quantum/classical gaps can be proven [2–9]. By contrast, exponential quantum/classical gaps for computation tasks such as factorization [10] depend on the best-known classical algorithm, and thus are strongly believed but not rigorously proven. Experimentally, quantum communication complexity has been studied in proof of principle for the quantum fingerprinting protocol [11–13] and beyond [1, 14, 15].

The quantum switch provides a new communication complexity tool that leads to another instance of exponential quantum advantage [16]. The quantum switch is a device where a control qubit determines the order in which two transformations are performed on a target system [17, 18]. When the control is in a superposition of logical states, the order of the operations is causally indefinite, i.e. there is a superposition of the ordering of target operations. The quantum switch has broad relevance in the context of quantum causality [19] including applications to studies of quantum gravity [19–22], communication complexity [16, 23], witnessing causality [17, 24–28] and deciding whether a given indefinite causal order is physical [29, 30]. In quantum computing, the quantum switch can reduce the query complexity for some tasks compared to causally ordered protocols [18, 31] — this advantage has been demonstrated for single-qubit control and single-qubit target circuits [32]. In quantum communication, the quantum switch enhances the communication rate beyond the limits of conventional quantum Shannon theory [33, 34].

In this work, we demonstrate a quantum-switch-based exponentially-enhanced quantum-communication protocol, modified from a recent theory proposal [16]. We implement a single-qubit-controlled switch acting on a target Hilbert space of d dimensions realized as a qudit [35, 36], which simplifies the experiment compared to using multiple qubits while maintaining the Hilbert-space dimension. Unlike past experimental qubit implementations [22, 26, 27, 32, 34], our experiment provides the first demonstration of the quantum switch involving a qudit target system.

The communication task that we consider is known as the exchange evaluation game, illustrated in Fig. 1. For bit strings $\mathbf{x}, \mathbf{y} \in \{0, 1\}^n$ and Boolean functions $f, g : \{0, 1\}^n \rightarrow \{0, 1\}$, Alice and Bob receive inputs (\mathbf{x}, f) and (\mathbf{y}, g) , respectively, such that $f(\mathbf{0}) = g(\mathbf{0}) = 0$, with $\mathbf{0}$ being the all-zero string. Another party, Charlie, must compute the exchange

evaluation function $EE(\mathbf{x}, f, \mathbf{y}, g) = f(\mathbf{y}) \oplus g(\mathbf{x})$ subject to the one-way communication condition that Alice and Bob can each send a system to the outside environment only once. They are thus forbidden to communicate back and forth by sending quantum or classical systems to each other at different time steps.

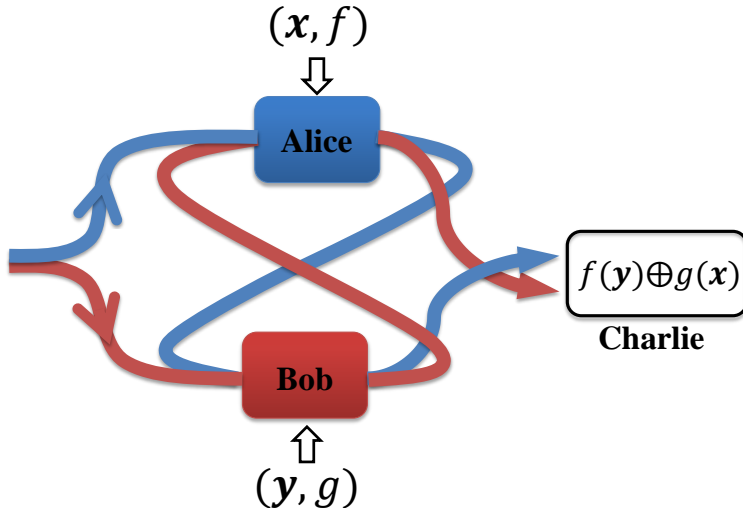


FIG. 1. Schematic illustration of the exchange evaluation game. Alice and Bob receive inputs (\mathbf{x}, f) and (\mathbf{y}, g) , respectively. There is another party, Charlie, who needs to compute the exchange evaluation function $EE(\mathbf{x}, f, \mathbf{y}, g) = f(\mathbf{y}) \oplus g(\mathbf{x})$. Under the condition of one-way communication, for a causally ordered protocol, Alice and Bob can transmit information either from Alice to Bob, then Charlie (blue arrow) or from Bob to Alice, then Charlie (red arrow). Using a quantum switch which creates a superposition of the communication direction, they solve the game with exponential advantage in the scaling of the required communication compared to any causally ordered protocol.

Guérin et al. proposed a protocol that uses the superposition of the communication direction between Alice and Bob to solve the exchange evaluation game with unit success probability, using an amount of communication that scales exponentially better with the input bit string size n compared to any causally ordered protocol [16]. They cast the task in terms of the problem of deciding whether two unitary operations, which depend on the inputs of Alice and Bob, commute or anticommute. This constitutes precisely the question that can be solved efficiently with the quantum switch. Importantly, the communication complexity advantage is not limited to the ideal case of deterministic answers, which are unachievable in any real experiment; it also survives for the more practical bounded-error

case. Despite the elegance of the protocol in theory, it is challenging in experiment as the protocol typically requires the manipulation of more than 10 entangled qubits to enter the regime where the causally indefinite advantage starts.

We implement a variant of the protocol that renders it experimentally feasible with current technology (see Appendix A and B). In our protocol, we use a quantum switch where one qubit acts as the control, and the target system is a d -dimensional qudit [35] with $d = 2^{n+1}$, thus making it equivalent to $(n+1)$ entangled qubits. We implement both systems with a single photon by encoding the control system in the path degree of freedom and the target system in the arrival time of the photon, which is divided into a set of 2^{n+1} time bins forming the basis $\{|z\rangle; z \in \{0, 1, \dots, 2^{n+1} - 1\}\}$. Consistent with the notation for z , we write x and y as the unary representations of the bit strings \mathbf{x} and \mathbf{y} , respectively, noting that the maximum value they can take is $2^n - 1$. To account for the different dimensionality of the target system and these bit strings, we trivially augment the functions f and g as $f(z) = g(z) = 0$ for $z \in \{2^n, 2^n + 1, \dots, 2^{n+1} - 1\}$.

Our protocol tests whether two unitary operators U_A and U_B commute or anti-commute when applied to a particular target state. The relationship between this task and the communication complexity one (evaluating $f(y) \oplus g(x)$) can be seen by representing U_A and U_B in the unitary-operator basis given by the generalized Pauli operators [35, 36] $X_d |z\rangle = |z + 1 \pmod d\rangle$ and $Z_d |z\rangle = \exp(2\pi iz/d) |z\rangle$ satisfying $Z_d X_d = \exp(2\pi i/d) X_d Z_d$. In this basis, we write $D_d(f) |z\rangle = Z_d^{f(z)d/2z} |z\rangle$ and define $U_A \equiv X_d^x D_d(f)$ and $U_B \equiv X_d^y D_d(g)$. Thus,

$$[U_A, U_B] |0\rangle_t = 0 \text{ if } f(y) \oplus g(x) = 0, \{U_A, U_B\} |0\rangle_t = 0 \text{ if } f(y) \oplus g(x) = 1; \quad (1)$$

where t denotes the target system.

The quantum switch can be used to solve this problem as follows. The control qubit is prepared in the state $|+\rangle_c = 1/\sqrt{2}(|0\rangle_c + |1\rangle_c)$, and the target system is initialized in $|0\rangle_t$. After applying the unitary operators U_A and U_B to the target system in the order determined by the control qubit, a Hadamard gate is applied to the control qubit, with the resulting state of the overall system being $\frac{1}{2}(|0\rangle_c \otimes \{U_A, U_B\} |0\rangle_t - |1\rangle_c \otimes [U_A, U_B] |0\rangle_t)$. Then, a measurement of the control qubit by Charlie in the computational basis reveals whether $f(y) \oplus g(x) = 0$ or $f(y) \oplus g(x) = 1$, which completes the communication-complexity task.

To implement the protocol, the state preparation and the Hadamard gate for the control

qubit encoded in the path degree of freedom are realized using a beam splitter (BS). The target qubit initialization in $|0\rangle_t$ is equivalent to the photon starting in the first time bin. The transformations $X(x) = X_d^x$ and $X(y) = X_d^y$ are implemented as delays by x time bins in Alice’s laboratory and y time bins in Bob’s laboratory, respectively. Furthermore, $D_d(f)$ is implemented in Alice’s laboratory using a phase modulator that applies the appropriate phase (0 if $f(z) = 0$ or π if $f(z) = 1$) to each time bin, with a corresponding implementation for $D_d(g)$ in Bob’s laboratory.

The experiment utilizes a fiber-based Sagnac interferometer, shown in Fig. 2. A heralded single photon, generated by type-II spontaneous parametric down-conversion (SPDC), passes a circulator and then enters the Sagnac loop, via a BS, in a superposition of two directions. Alice and Bob each possess a variable delay line and a time-dependent phase modulator (PM) to realize the unitary transformations U_A and U_B , respectively. They each implement the transformation once on the component of the photon that passes through them after entering the loop, and once more on the component that passes through them before exiting the loop. Depending on the binary answer to the exchange evaluation game, the photon interferes such that it exits at one or the other of the two interferometer outputs. The outputs are monitored by two high-quality superconducting nanowire single-photon detectors (SNSPDs). The detection events are registered using a time-to-digital converter (TDC).

In the experimental implementation of the communication complexity protocol, the amount of communication and the error probability are to be minimized. These goals lead to three main technological challenges (see Appendix C). (i) Precise timing is required to ensure that the correct phase is imparted at the second station. We use a sequence of home-made fiber segments to create the 2^n choices of delays for each of Alice and Bob with a high accuracy, and a 25 GHz arbitrary waveform generator, triggered by the heralding signal, in such a way that the modulation timing accurately coincides with the time bins (of length 2 ns) of the heralded photons. (ii) To minimize noise, we use two SNSPDs with ultra-low dark-count rates below 10 Hz, and perform careful temperature control and polarization control to maximize the interference visibility. (iii) It requires the optimization of the efficiency throughout the set-up, to minimize the amount of required communication. For example, we need a loss < 15.94 dB to beat the classical definite protocol with $n = 10$. To this end, we choose suitable pump and detection beam waists for the down-conversion process, use custom-made low-loss components in the Sagnac loop, and detect the photons

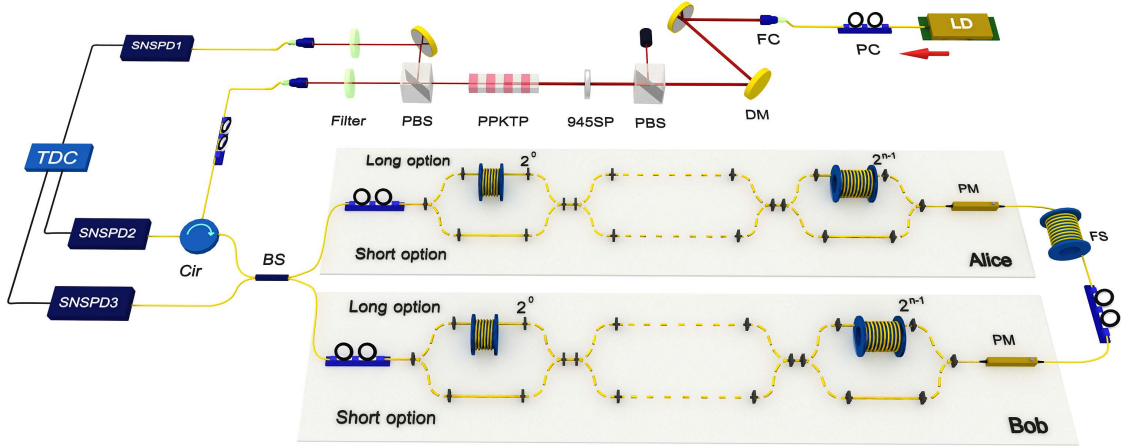


FIG. 2. Experimental set-up of the causally indefinite protocol. The pump light is emitted by a 780 nm continuous-wave laser diode (LD). After passing through a 945 nm short-pass filter (945SP) used to remove the residual long wavelengths from outside fluorescence, the pump light is focused into a 10 mm, periodically poled potassium titanyl phosphate (PPKTP) crystal to convert pump photons into pairs of orthogonally polarized photons at a wavelength of 1560 nm. The down-converted photons are separated by a polarizing beam splitter (PBS), and the residual pump photons are removed by two filters. One of the down-converted photons is sent to a circulator (Cir) and then enters the Sagnac loop via a beam splitter (BS). To herald the presence of this photon, the other one is directly detected by a high-quality superconducting nanowire single-photon detector (SNSPD1). In the Sagnac loop, Alice and Bob each possess a variable delay and a phase modulator (PM) to implement their unitary transformations. For each of the n segments, either the long option or the short option is chosen, depending on whether the corresponding digit of x in binary representation is 0 or 1. A fiber spool (FS) with a length of 7 km is used to store the pulse train. The interference results are monitored by SNSPD2 and SNSPD3. Abbreviations of other components: PC, polarization controller; FC, fiber coupler; DM, Dichroic Mirror; TDC, time-to-digital converter.

with high-efficiency SNSPDs.

In our experiment, we determine the error probability and the transmitted information for each $n \in \{9, 10, 11, 12\}$. We record two-photon coincidence counts (between SNSPD1 and either SNSPD2 or SNSPD3; Fig. 2). We estimate the error probability ϵ (i.e. the probability of an incorrect result) focusing on two important cases: the worst case, where

both Alice and Bob have the largest input $x = y = 2^n - 1$ (corresponding to the largest delays and system loss); and the one-bit-different case where Alice changes the choice of the $(k + 1)$ -th segment, $k \in \{0, 1, 2, \dots, n - 1\}$, while Bob holds the largest input. The goal of testing the second case is to verify that the delay of each segment is well made, so that Alice has the ability to implement any of the 2^n possible delays. Figure 3 shows the detailed experimental error probability for $n = 12$, where we obtained a value of $\epsilon = 0.0638 \pm 0.0025$ for the worst case (red bar). As expected, for other values of k , the error probability is below that of the worst case. For other values of n , see Appendix D.

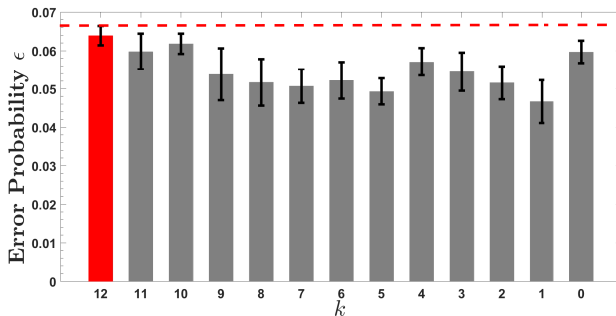
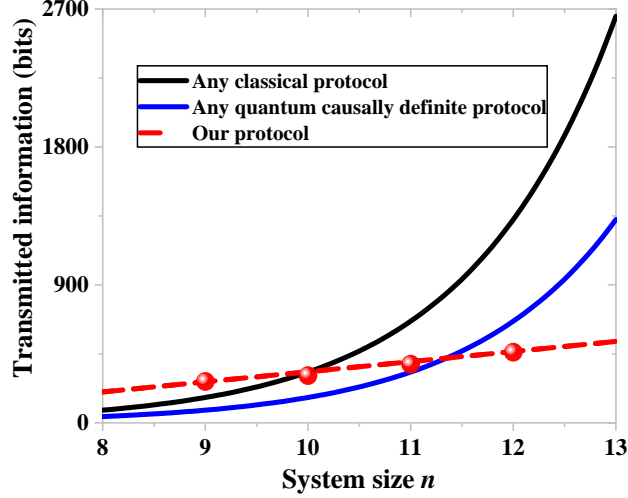
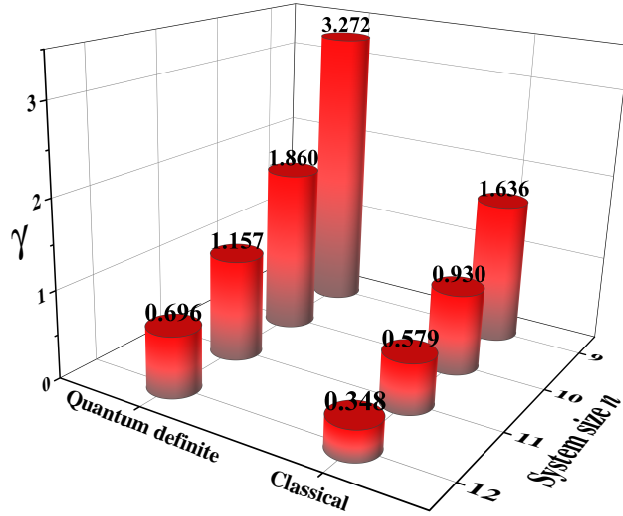


FIG. 3. (Color online) Error probability for the system size $n = 12$. The value $k = 12$ denotes the worst case of inputs $x = y = 2^n - 1$. The other values of $k \in \{0, 1, \dots, 11\}$ correspond to Alice’s $(k + 1)$ -th bit being flipped from 1 to 0. The red dashed line shows the worst error probability including the uncertainty. The error bars indicate one standard deviation.

Figure 4(a) shows the experimental transmitted information required to complete the task for different system sizes. We compare our protocol with a bound for classical protocols (black solid curve) and a bound for quantum causally definite protocols (blue solid curve). A lower bound on the transmitted information in any classical protocol, allowing for a bounded error probability of ϵ , is $(1 - H(\epsilon))2^{n-1}$, where $H(\epsilon)$ is the binary entropy. Any quantum causally definite protocol needs to transmit at least $(1 - H(\epsilon))2^{n-2}$, half as much as classical protocols [16]. We use the worst-case ϵ ($= 0.0663$) to calculate the minimum transmitted information of classical and quantum causally definite protocols, because it gives the most stringent bound to beat. For each n , the transmitted information of our protocol is estimated to be $(n + 2)/\eta_n$, where η_n ($n \in \{9, 10, 11, 12\}$) denotes the worst-case overall system efficiency for the given system size. Figure 4(a) indicates that, with increasing system size n , the causally indefinite protocol provides an exponential advantage in the scaling of



(a)



(b)

FIG. 4. (a) Comparison of the transmitted information. The red points show our experimental results for different system sizes. The red dashed line is the best fit straight line for the four data points. The error bars are too small to be seen. For $n = 12$ our experimental result clearly beats both classical protocols and quantum causally definite protocols. (b) The ratio γ of the transmitted information Q of our causally indefinite protocol, and the lower bound on the transmitted information C for a given causally ordered protocol.

transmitted information. In particular, for $n = 12$, the experimental results clearly beat all classical protocols as well as all quantum causally definite protocols.

To further quantify our results, we define γ as the ratio between the transmitted infor-

mation Q of our causally indefinite protocol, and the minimum transmitted information C of a given type of causally ordered protocol (either classical or quantum causally definite): $\gamma := Q/C$. In figure 4(b), we plot the experimental results for γ as a function of different protocols and different input sizes. Figure 4(b) shows that our protocol requires the transmission of only $(34.8 \pm 0.3)\%$ of the information of any classical protocol and $(69.6 \pm 0.6)\%$ of the information of any causally definite quantum protocol.

Overall, we have experimentally demonstrated that the superposition of communication direction can provide an exponential reduction of communication complexity. We achieve this through the use of a high-dimensional degree of freedom, the photon arrival time. Although our temporal qudit encoding is not efficiently scalable to very large n , our experiment elucidates the crucial role of coherence in achieving the exponential separation between quantum and classical communication in a distributed processing task. Decoherence would destroy the superposition of communication directions—reverting to a situation where it is necessary to transmit the function itself through the one-way channel to achieve deterministic two-party function evaluation. Our results establish that the quantum switch can serve as a powerful resource in quantum communication, which may provide a new paradigm of Shannon theory, where the order of the communication channels can be in a quantum superposition, and therefore strongly motivates further experimental development with qudit or other encodings.

ACKNOWLEDGMENTS

This work was supported by Fundamental Research Funds for the Central Universities (WK2340000083), National Key R&D Program of China (SQ2018YFB050101), the National Natural Science Foundation of China (Grant No. 61771443 and No. 61705048), the Chinese Academy of Sciences, the Thousand Young Talent Program of China, Shanghai Science and Technology Development Funds (18JC1414700), and the Australian Research Council Grant No. DP160101911. The authors would like to thank Norbert Lütkenhaus, Farzad Ghafari, Jian-Yu Guan and Cheng Wu for helpful discussions.

Appendix A: Comparison of our protocol with that of Ref. [16]

Our protocol differs slightly from the original scheme proposed in Ref. [16]. The unitary transformation $X(\mathbf{x})$ was originally proposed in terms of modulo-two addition, as $X(\mathbf{x}) = \sum_{\mathbf{z} \in \{0,1\}^n} |\mathbf{z} \oplus \mathbf{x}\rangle\langle\mathbf{z}|$. Our definition of $X(x) = \sum_z |(z+x) \bmod 2^{n+1}\rangle\langle z|$ retains the key property of $[X(x), X(y)] = 0 \forall x \text{ and } y$, while being experimentally much more readily realizable. Note that the fact that our target system is equivalent to $n+1$ qubits as opposed to the n qubits of Ref. [16] is not a fundamental consequence of the time-bin implementation. One could also have the target system corresponding to n qubits, and use the transformation $X(x) = \sum_{z=0}^{2^n-1} |(z+x) \bmod 2^n\rangle\langle z|$. Such a permutation would require using fast switches in addition to the delays, as shown in Fig. 5.

Appendix B: Practical considerations

Our encoding of the whole multi-qubit system in a single photon entails both benefits and drawbacks. It is beneficial given the presence of probabilistic photon loss, an unavoidable experimental imperfection. Efficiency is a crucial factor in demonstrating the advantage provided by the quantum switch, and presents one of the main technical challenges of the experiment. Loss is detrimental because it effectively requires the repetition of the protocol, thereby increasing the communication, while the performance is benchmarked against optimal lossless causally ordered protocols. As a result of our implementation, our quantum system is only subjected to the probabilistic loss associated with one photon. However, the encoding of the target qubits in the photon arrival time also leads to an exponential growth of the number of required time bins as a function of the number of target qubits. This practically limits the ability to scale the protocol to an arbitrarily high value of n . Nevertheless, our experiment proves that it is possible to access the regime where our causally indefinite quantum protocol outperforms any causally definite protocol.

In contrast to previous communication complexity experiments on quantum fingerprinting that were based on coherent states [12, 13], we use single photons in this experiment. The use of coherent states would arguably violate a rule of the exchange evaluation game, namely that Alice and Bob are each only allowed to receive a system from the outside environment once. As a test of one-way communication, Ref. [16] proposed having a (hypothetical) counter

in each laboratory that is incremented by one whenever a system enters the laboratory. Our single photon constitutes an indivisible quantum system, so the meaning of “a system entering” is unambiguous, and the counters would read one at the end of the protocol, in agreement with the rules of the game. However, for the case of a coherent state divided on a beam splitter, each component could be considered a quantum system on its own. In that case, the counters would read two, in violation of the rules of the game. It has recently also been experimentally shown that the use of single photons can enable secure communication with a hidden communication direction [37].

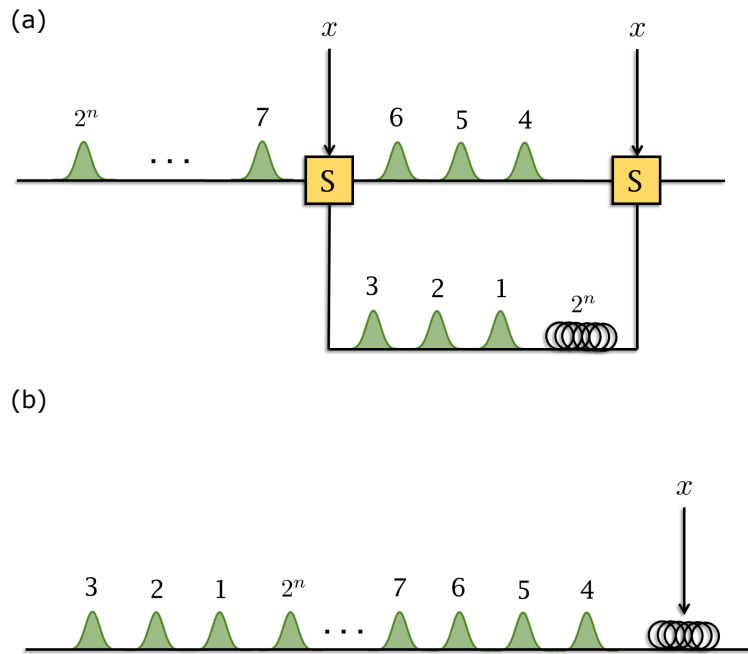


FIG. 5. Linear optic circuit for performing an alternative version of the transformation $X(x)$, such that the number of qubits in the target system is reduced to n . (a) The 2^n incoming modes pass through an active switch S which sends each mode either straight through or sends it to a delay line. The delay is equivalent to 2^n time bins. The operation of the switch depends on x and it is such that only the first $(2^n - x)$ modes are sent through the delay. Here we have used $x = 2^n - 3$ as an example. A second switch then ensures that all modes exit in the same line. (b) After the previous step, the modes have been permuted as desired and an further delay equal to x time bins must be added to ensure that the leading mode reaches the other party at the same time, regardless of the value of x .

Appendix C: Experimental details

1. Heralded single-photon source

The photon pairs are produced via type-II spontaneous parametric down-conversion. The pump light is emitted by a 780 nm continuous-wave laser diode (LD). After passing through a 945 nm short-pass filter (945SP) used to remove the residual long wavelengths from outside fluorescence, the pump light is focused into a 10 mm, periodically poled potassium titanyl phosphate (PPKTP) crystal to convert pump photons into pairs of orthogonally polarized photons at a wavelength of 1560 nm. The down-converted photons are separated by a polarizing beam splitter (PBS), and the residual pump light is removed by two filters. The down-converted photons are then coupled into single-mode fibers with a 76.9% coupling efficiency. One of them passes a circulator before entering the Sagnac loop. To herald the presence of the correlated photon, the other one is directly detected by a high-quality superconducting nanowire single-photon detector (SNSPD1) with 80.6% detection efficiency. Overall, the heralding efficiency is approximately $(62.0 \pm 1.0)\%$, including all losses in the photon-pair source set-up (but excluding the elements used to implement the communication complexity protocol).

2. Sagnac loop

The Sagnac loop is depicted in Fig. 2 of the main text. A 50:50 beam splitter (BS) is used to create the superposition of communication direction. Alice and Bob each possess a variable delay and a phase modulator to implement their unitary operators based on their inputs when the photon arrives at their stations. The unitaries consist of phase modulations followed by delays. However, because $f(0) = g(0) = 0$ and the photon is initialized in the first time bin, no phase modulation needs to be implemented at the first station, only the delays. The photon then continues along the Sagnac loop, through a 7 km fiber spool in which the pulse trains are stored, and to the second station. There, Alice and Bob each implement their phase modulation, followed by their delay. Finally, the two paths interfere at the BS and the photon is detected by two high-quality SNSPDs (SNSPD2 with a detection efficiency of 76.5% and dark count rate of 9.3 Hz, SNSPD3 with a detection efficiency of 72.0% and a dark count rate of 8.3 Hz). The two-photon coincidences are registered by a

time-to-digital converter (TDC). All components in the loop have ultra-low insertion loss to minimize the communication complexity.

3. Dark counts

The coincidence time window in the causally indefinite protocol is very large. In contrast to typical two-photon coincidence experiments where the coincidence window tends to be a few ns, in the causally indefinite protocol, the heralding photon arrives in a given time bin while the heralded photon can be in one of 2^{n+1} time bins. This means that the coincidence time window is 2^{n+2} ns for the given 2 ns time bin, $\sim (n + 1)/3$ orders of magnitude larger than that in normal two-photon coincidence detection. If there is a dark count during this time (or a subset of this interval when applying gating), it will be erroneously registered as an event. To suppress dark counts due to thermal background radiation, we use two high-quality SNSPDs that use a low-loss bandpass filter. The SNSPDs can detect photons with an ultra-low dark-count rate of < 10 Hz and a high detection efficiency of $> 72.5\%$.

4. Losses

To minimize the experimental communication in the causally indefinite protocol, the experimental set-up should have as small a loss as possible. Here, three strategies are applied to minimize the total loss of the set-up. First, for the heralded single-photon source, by setting the pump beam waist to $340 \mu\text{m}$, the detection beam waist at the center of the PP-KTP crystal to $170 \mu\text{m}$, and by heralding the daughter photons using a high-quality SNSPD (detection efficiency of 80.6% , dark count rate of 11.0 Hz), we achieve a high heralding efficiency of $(62.0 \pm 1.0)\%$, corresponding to 2.07 dB loss in the source. Second, in the Sagnac loop, all components are custom-made to achieve ultra-low loss. As discussed in subsection 5 of this section, instead of using highly lossy optical switches, we implement the delay by joining the different fiber segments via mating sleeves. There, we use different connector types, SC/PC to FC/PC mating sleeves (Thorlabs), which provide a lower loss (< 0.11 dB), compared with a typical loss of FC/PC to FC/PC mating sleeves (~ 0.3 dB). As a result, for each system size n , we implement the delays with extremely low loss. Lastly, for the detection we use two high-quality SNSPDs that have a high detection efficiency of 72.0%

and 76.5% together with an ultra-low dark count rate of 8.3 Hz and 9.3 Hz, respectively. The overall system loss, excluding the loss of the variable delays in Alice and Bob’s stations, is 11.66 dB.

5. Implementation of the unitary transformations

For our protocol, Alice (Bob) needs to realize one of the 2^n possible delays, depending on her (his) input bit string, and guarantee that her (his) PM correctly modulates the photon after the delay from Bob (Alice). Therefore, after the delay, the photon pulse must be fully contained in the appropriate time bin. Instead of using highly lossy switches, we implement the variable delays with n segments of fiber, where for the k -th segment, there is a choice of two fibers that have a length difference equivalent to a delay of 2^{k-1} time bins, $k \in \{1, 2, \dots, n\}$, as illustrated in Fig. 6. We use a 25 GHz arbitrary waveform generator (Tektronix70002), which is triggered by the heralding signal, to generate a modulation pulse sequence with a pulse width of 2 ns. The rising edge and the falling edge of the pulse are < 100 ps. The delay between the heralding signal and the modulation pulse is accurately controlled such that the heralded photon is positioned in the middle of the first time bin.

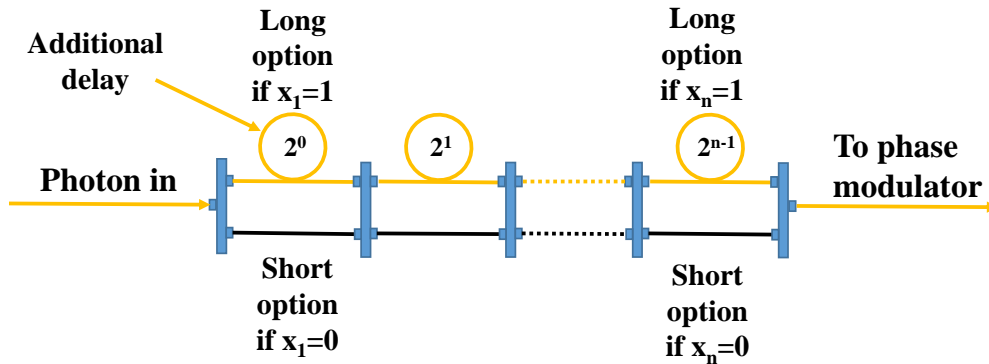


FIG. 6. (Color online) Schematic of the implementation of $X(x)$. For each of the n segments, either the short option (black fiber) or the long option (yellow fiber) is chosen, depending on whether the corresponding digit of x in binary representation is 0 or 1. For the k -th segment, the length of the long option and that of the short option are $t \times (2^{k-1} + 1)$ and t , respectively, where $t = 2$ ns is the pulse width of phase modulation.

The time delay of commercial off-the-shelf fiber spools is measured using a conventional optical time domain reflectometer (OTDR). By itself, it has a low accuracy and does not

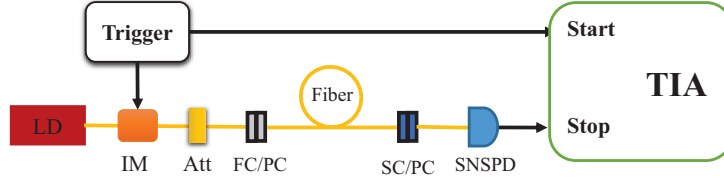


FIG. 7. (Color online) Set-up of the delay measurement. We use a continuous-wave laser diode (LD) at 1560 nm, an intensity modulator (IM), and an attenuator (Att) to generate pulse signals with a temporal width of ~ 100 ps. Then we acquire the two arrival-time distributions of the photons after travelling through the fiber segments of interest, using an SNSPD and a time interval analysis (TIA, Picoquant HydraHarp400). The delay of the fiber spool is calculated as the difference of the mean values of the two distributions. Since the IM and the start of the TIA are triggered by the same electronics, the same detector is used for both distributions, and we use the time-tag unit, the difference is only affected by the resolution of the TIA, reaching 1 ps.

meet the sensitivity demands of our experiment. For example, the distance uncertainty of a conventional state-of-the-art OTDR (Exfo FTB7600E) is $\pm(0.75 + 0.001 \times L)$ meter, corresponding to a time-delay uncertainty of $\pm(3.75 + 0.001 \times L/v)$ ns, where L is the length of the fiber spool and v is group velocity in fiber. In our experiment, we home made all the fiber segments with a time-delay uncertainty of ~ 2.5 ps using the following method:

1. To make one of the segments whose time delay is $2 \times (2^{k-1} + 1)$ ns, we cut off a $2 \times (2^{k-1} + 1) + 5$ ns time-delay fiber with an FC/PC connector at one end and an SC bare fiber terminator (Thorlabs) at the other end, using a commercial OTDR to approximate the length. For the segments whose time delay is in the event dead zone of the OTDR, we directly make it by using a ruler with a resolution of 0.5 mm (= 2.5 ps).
2. We measure the time delay of the segment using our home-built photon-counting OTDR variant shown in Fig. 7, which achieves a resolution of 1 ps. Then, we cleave the redundant fiber whose length is measured by a ruler with a resolution of 0.5 mm (= 2.5 ps).
3. We pull the fiber out the bare fiber terminator. Then the fiber is connectorised and is slightly polished with an SC/FC connector achieving a low insertion loss.

The resultant length of each of the fiber segments for Alice and Bob is shown in Table I. For different combinations of fiber segments, the largest deviation of the delay, compared to the target value, is 101 ps for Alice and 46 ps for Bob—both of which are far below 900 ps (the maximum deviation of the delay if we want to apply the correct phase to the photon pulse in the desired time bin).

TABLE I. (a) Length of each of Alice’s fiber segments. (b) Length of each of Bob’s fiber segments. For the k -th segment, the length of the long option and that of the short option are $t \times (2^{k-1} + 1)$ and t , respectively, where $t = 2$ ns is the pulse width of phase modulation. Errors shown represent one standard deviation.

(a)

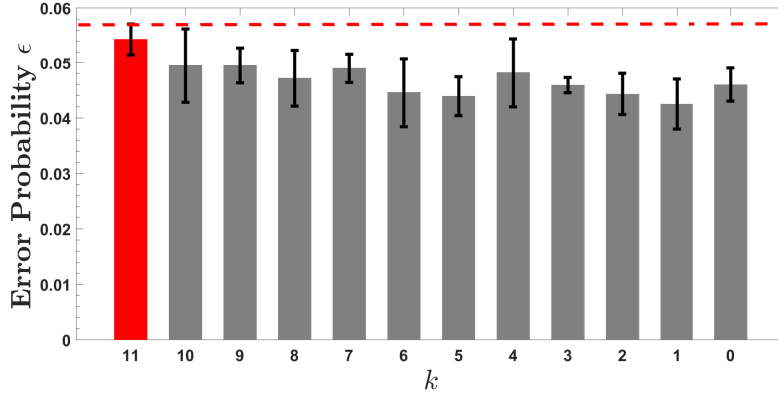
	k	1	2	3	4	5	6
Option							
Long (ns)		4.006 ± 0.001	6.007 ± 0.001	10.004 ± 0.000	18.012 ± 0.001	33.999 ± 0.002	66.002 ± 0.001
Short (ns)		2.008 ± 0.001	2.010 ± 0.001	2.008 ± 0.001	2.008 ± 0.001	2.010 ± 0.001	2.003 ± 0.001
	k	7	8	9	10	11	12
Option							
Long(ns)		130.008 ± 0.001	257.948 ± 0.001	513.995 ± 0.001	1025.985 ± 0.001	2049.936 ± 0.002	4098.000 ± 0.005
Short(ns)		2.003 ± 0.001	2.009 ± 0.001	2.006 ± 0.001	2.009 ± 0.001	2.009 ± 0.001	2.008 ± 0.001

(b)

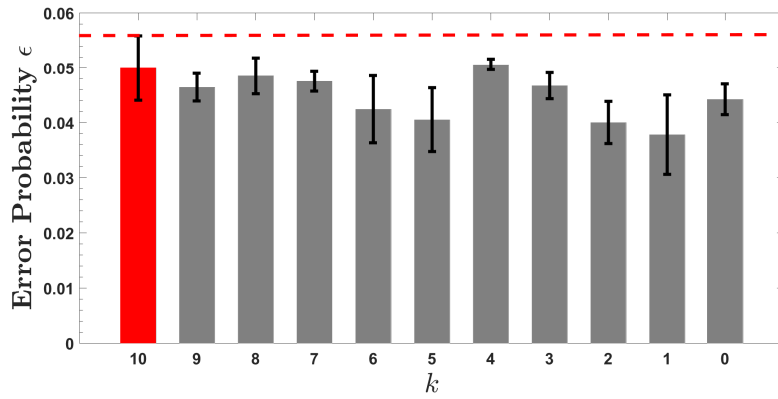
	k	1	2	3	4	5	6
Option							
Long (ns)		4.013 ± 0.001	6.010 ± 0.001	10.003 ± 0.001	18.004 ± 0.001	34.009 ± 0.000	66.056 ± 0.001
Short (ns)		2.008 ± 0.001	1.999 ± 0.001	2.008 ± 0.001	2.009 ± 0.001	2.007 ± 0.001	2.010 ± 0.001
	k	7	8	9	10	11	12
Option							
Long (ns)		130.002 ± 0.001	257.992 ± 0.001	514.004 ± 0.001	1025.999 ± 0.002	2049.961 ± 0.004	4097.993 ± 0.007
Short (ns)		2.005 ± 0.001	2.006 ± 0.001	2.005 ± 0.001	2.004 ± 0.001	2.007 ± 0.001	2.002 ± 0.001

Appendix D: Detailed Experimental results

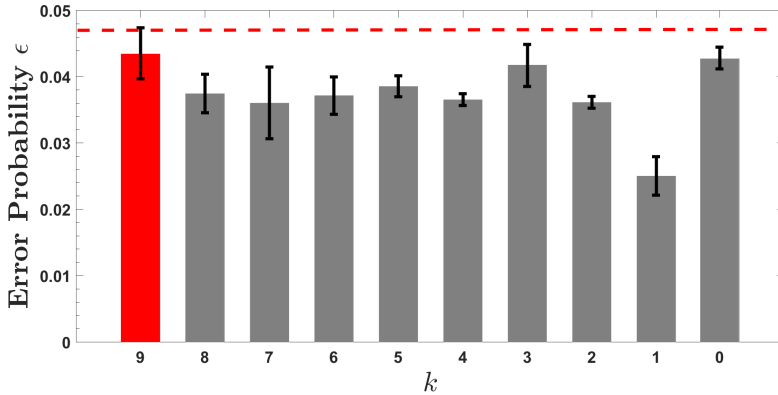
Table II shows the complete experimental results. Figure 8 shows the experimental error probabilities of different system sizes ranging from $n = 11$ to 9. For each system size, the largest error probability is obtained in the worst case (red bar). The error bars represent one standard deviation.



(a)



(b)



(c)

FIG. 8. (a) Error probability for the system size $n = 11$. (b) Error probability for the system size $n = 10$. (c) Error probability for the system size $n = 9$. For each system size n , the red bar denotes the worst case of inputs $x = y = 2^n - 1$. The other values of $k \in \{0, 1, \dots, 11\}$ correspond to Alice's $(k + 1)$ -th bit being flipped from 1 to 0. The red dashed line illustrates the worst error probability accounting for the uncertainty. The error bars indicate one standard deviation.

TABLE II. Detailed experimental results. The system loss and the error probability are estimated for the worst-case inputs for Alice and Bob (consisting of $x = y = 2^n - 1$ and $f(z) = g(z) = 0$ for z even and $f(z) = g(z) = 1$ for z odd). The error bars indicate one standard deviation.

System size (n)	9	10	11	12
System loss (dB)	13.86 ± 0.04	14.06 ± 0.04	14.66 ± 0.04	15.14 ± 0.04
Error probability (ϵ)	0.0405 ± 0.0023	0.0498 ± 0.0059	0.0543 ± 0.0028	0.0638 ± 0.0025
Q	271.26 ± 2.50	308.45 ± 2.84	383.66 ± 3.53	461.45 ± 4.25
γ (classical)	1.636 ± 0.015	0.930 ± 0.008	0.578 ± 0.005	0.348 ± 0.003
γ (quantum definite)	3.272 ± 0.030	1.860 ± 0.017	1.157 ± 0.010	0.696 ± 0.006

-
- [1] H. Buhrman, R. Cleve, S. Massar, and R. de Wolf, *Rev. Mod. Phys.* **82**, 665 (2010).
- [2] A. C.-C. Yao, in *Proceedings of the 11th Annual ACM Symposium on Theory of Computing* (ACM, New York, 1979) pp. 209–213.
- [3] G. Brassard, *Found. Phys.* **33**, 1593 (2003).
- [4] R. Raz, in *Proceedings of the Thirty-first Annual ACM Symposium on Theory of Computing*, STOC '99 (ACM, New York, 1999) pp. 358–367.
- [5] H. Buhrman, R. Cleve, J. Watrous, and R. De Wolf, *Phys. Rev. Lett.* **87**, 167902 (2001).
- [6] Z. Bar-Yossef, T. S. Jayram, and I. Kerenidis, in *Proceedings of the Thirty-sixth Annual ACM Symposium on Theory of Computing* (ACM, New York, 2004) pp. 128–137.
- [7] D. Gavinsky, J. Kempe, I. Kerenidis, R. Raz, and R. de Wolf, in *Proceedings of the Thirty-ninth Annual ACM Symposium on Theory of Computing*, STOC '07 (ACM, New York, 2007) pp. 516–525.
- [8] O. Regev and B. Klartag, in *Proceedings of the Forty-third Annual ACM Symposium on Theory of Computing*, STOC '11 (ACM, New York, 2011) pp. 31–40.
- [9] J. M. Arrazola and N. Lütkenhaus, *Phys. Rev. A* **89**, 062305 (2014).
- [10] P. W. Shor, *SIAM Review* **41**, 303 (1999).
- [11] R. T. Horn, S. A. Babichev, K.-P. Marzlin, A. I. Lvovsky, and B. C. Sanders, *Phys. Rev. Lett.* **95**, 150502 (2005).

- [12] F. Xu, J. M. Arrazola, K. Wei, W. Wang, P. Palacios-Avila, C. Feng, S. Sajeed, N. Lütkenhaus, and H.-K. Lo, *Nat. Commun.* **6**, 8735 (2015).
- [13] J. Y. Guan, F. Xu, H. L. Yin, Y. Li, W. J. Zhang, S. J. Chen, X. Y. Yang, L. Li, L. X. You, T. Y. Chen, Z. Wang, Q. Zhang, and J. W. Pan, *Phys. Rev. Lett.* **116**, 240502 (2016).
- [14] J. Du, P. Zou, X. Peng, D. K. Oi, L. C. Kwek, C. H. Oh, and A. Ekert, *Phys. Rev. A* **74**, 042319 (2006).
- [15] P. Trojek, C. Schmid, M. Bourennane, Č. Brukner, M. Żukowski, and H. Weinfurter, *Phys. Rev. A* **72**, 050305 (2005).
- [16] P. A. Guérin, A. Feix, M. Araújo, and Č. Brukner, *Phys. Rev. Lett.* **117**, 100502 (2016).
- [17] O. Oreshkov, F. Costa, and Č. Brukner, *Nat. Commun.* **3**, 1092 (2012).
- [18] G. Chiribella, G. M. D'Ariano, P. Perinotti, and B. Valiron, *Phys. Rev. A* **88**, 022318 (2013).
- [19] Č. Brukner, *Nat. Phys.* **10**, 259 (2014).
- [20] L. Hardy, *J. Phys. A Math. Theor.* **40**, 3081 (2007).
- [21] M. Zych, F. Costa, I. Pikovski, and Č. Brukner, [arXiv:1708.00248](https://arxiv.org/abs/1708.00248).
- [22] G. Rubino, L. A. Rozema, F. Massa, M. Araújo, M. Zych, Č. Brukner, and P. Walther, [arXiv:1712.06884](https://arxiv.org/abs/1712.06884).
- [23] A. Feix, M. Araújo, and Č. Brukner, *Phys. Rev. A* **92**, 052326 (2015).
- [24] M. Araújo, C. Branciard, F. Costa, A. Feix, C. Giarmatzi, and Č. Brukner, *New J. Phys.* **17**, 102001 (2015).
- [25] C. Branciard, M. Araújo, A. Feix, F. Costa, and Č. Brukner, *New J. Phys.* **18**, 013008 (2015).
- [26] G. Rubino, L. A. Rozema, A. Feix, M. Araújo, J. M. Zeuner, L. M. Procopio, Č. Brukner, and P. Walther, *Sci. Adv.* **3**, e1602589 (2017).
- [27] K. Goswami, C. Giarmatzi, M. Kewming, F. Costa, C. Branciard, J. Romero, and A. G. White, *Phys. Rev. Lett.* **121**, 090503 (2018).
- [28] E. Castro-Ruiz, F. Giacomini, and Č. Brukner, *Phys. Rev. X* **8**, 011047 (2018).
- [29] M. Araújo, A. Feix, M. Navascués, and Č. Brukner, *Quantum* **1**, 10 (2017).
- [30] O. Oreshkov, [arXiv:1801.07594](https://arxiv.org/abs/1801.07594).
- [31] M. Araújo, F. Costa, and Č. Brukner, *Phys. Rev. Lett.* **113**, 250402 (2014).
- [32] L. M. Procopio, A. Moqanaki, M. Araujo, F. Costa, I. Alonso Calafell, E. G. Dowd, D. R. Hamel, L. A. Rozema, Č. Brukner, and P. Walther, *Nat. Commun.* **6**, 7913 (2015).
- [33] D. Ebler, S. Salek, and G. Chiribella, *Phys. Rev. Lett.* **120**, 120502 (2018).

- [34] K. Goswami, J. Romero, and A. G. White, arXiv:1807.07383.
- [35] S. D. Bartlett, H. de Guise, and B. C. Sanders, Phys. Rev. A **65**, 052316 (2002).
- [36] J. Patera and H. Zassenhaus, J. Math. Phys. **29**, 665 (1988).
- [37] F. Massa, A. Moqanaki, F. Del Santo, B. Dakic, and P. Walther, arXiv:1802.05102.